Third sound and stability of thin ^{3}He-^{4}He films

E. Krotscheck* and M. D. Miller†
Institut für Theoretische Physik, Johannes-Kepler-Universität, A-4040 Linz, Austria
(Received 24 March 2005; revised manuscript received 9 January 2006; published 17 April 2006)

We study third sound in thin ^{3}He-^{4}He mixture films from first-principles, microscopic theory and compare these results to the usual film-averaged, hydrodynamic approach. The hydrodynamic approach yields third-sound speeds that depend only on the thickness of the superfluid film and the distribution of impurities—i.e., ^{3}He. In very thin films, this result clearly must be modified to account for the effects of nonuniform ^{4}He film density. Utilizing the variational, hypernetted-chain–Euler-Lagrange theory as applied to inhomogeneous boson systems, we calculate accurate chemical potentials for both the ^{4}He superfluid film and the physisorbed ^{3}He. Numerical density derivatives of the chemical potentials lead to the sought-after third-sound speeds that clearly reflect a layered structure of at least seven oscillations. We are thus able to gauge the range of applicability of the film-averaged hydrodynamic results as applied to thin quantum liquid films. We study third sound on two model substrates: Nuclepore and glass. We compute the change in third-sound speed as a function of ^{3}He coverage in the linear (low-concentration) regime, which is then studied for the two substrates as a function of ^{4}He film thickness and compared to existing experiments.^{3}He density profiles are calculated as a function of ^{4}He film thickness, and we show explicitly the smooth transition from Andreev states in the thick-film limit to lateral mixtures in the submonolayer limit. This effect was first seen by Noiray *et al.* [Phys. Rev. Lett. **53**, 2421 (1984)]. Our results predict that the addition of a small amount of ^{3}He can increase, as well as decrease, the third-sound speed relative to that of the pure ^{4}He film. Further, we show that the addition of a small amount of ^{3}He can destabilize the film and drive a phase separation into lateral regions of ^{3}He-rich and ^{3}He-poor patches. This latter result may help explain the phase transitions reported by Bhattacharyya and Gasparini [Phys. Rev. Lett. **49**, 919 (1982)] and Csáthy, Kim, and Chan [Phys. Rev. Lett. **88**, 045301 (2002)] in thin mixture films.

DOI: 10.1103/PhysRevB.73.134514 PACS number(s): 67.70.+n, 67.60.Fp, 64.30.+t

I. INTRODUCTION

Using a *film-averaged*, hydrodynamical approach developed by Bergman[1] in his theory of third sound in ^{4}He films, it was shown in Refs. 2 and 3 that, in the low-temperature limit, the third-sound speed in a double-layer mixture film can be written as

$$\left(\frac{c_3^2}{c_{30}^2}\right) = 1 - \frac{\rho_u}{\rho_\ell}\left[\frac{f_u(h_\ell) - f_u(h_\ell + h_u)}{f_\ell(h_4^0)}\right], \tag{1.1}$$

where the quantity $c_{30}^2 = -(h_4 - h_0) f_\ell(h_4^0)$ is the third-sound speed for pure ^{4}He. The ℓ and u subscripts correspond to the lower and upper layers. Both the upper and lower films can, in principle, be mixtures of the ^{4}He and ^{3}He components. The ρ's are film-averaged mass densities, h_ℓ is the height of the mobile film above the substrate, and h_0 is the thickness of the immobile ^{4}He layer next to the substrate. The force functions $f_x(h)$ describe the interaction of the substrate on the film surfaces. They are taken to be in van der Waals form

$$f_x(h) = -\frac{3\alpha_s}{m_x h^4}, \tag{1.2}$$

where α_s is the substrate-helium van der Waals constant, $x = \{\ell, u\}$, and m_x are film-averaged masses. This approach is valid for films that can be characterized by a single thickness parameter h_ℓ, h_u, or h_4^0. Equation (1.1) can be utilized in different limits by assuming different behavior for the quantities h_ℓ, ρ_ℓ, h_u, and ρ_u as a function of ^{3}He coverage. In the literature, Eq. (1.1) has been successfully used to describe the third-sound response for both multilayer ^{4}He films[2,3] and thin ^{4}He films.[4]

As with thermodynamics, hydrodynamics requires material-specific information in order to provide output data. In the case of a very inhomogeneous system, such as ^{3}He adsorbed in a thin ^{4}He film, this input can be both ambiguous and complicated. The third-sound speed in a mixture film will depend both on the structure of the ^{4}He film and the distribution of ^{3}He in and on the film surface. The ^{3}He distribution itself depends on the occupation of single-particle surface states.[4] At low coverages the ^{3}He will occupy the ground state; however, with increasing coverage the ^{3}He may start occupying the first excited state and the changed spatial distribution leads to a changed third-sound response.

In this paper, we shall concentrate on two-mixture-third-sound experiments on Nuclepore and glass substrates as reported by Hallock and co-workers. The first, by Sheldon and Hallock,[5] was on a Nuclepore substrate. We refer the reader to Ref. 5 and references cited therein for a discussion of the experimental details. For this system, the film thickness h_4^0 is 13.2 Å. The substrate, Nuclepore, is a polycarbonate material threaded with pores of nominal diameter ≈2000 Å. The low-coverage results are linear and can be represented by

$$\frac{c_3^2}{c_{30}^2} \simeq 1 - \Delta\theta_3, \tag{1.3}$$

where $\theta_3 = (\sigma_3/\sigma_{3\ell})$ is the coverage in units of monolayers and $\sigma_{3\ell} \equiv 1/\ell_3^2$ is the areal density at "conventional" mono-

TABLE I. A comparison of the Nuclepore and glass substrates. ℓ_4=3.6 Å is the conventional ^{4}He single layer.

	Type	Immobile layer (h_0) (ℓ_4)	van der Waals (α_s) (K Å^3)
Nuclepore	Amorphous	2.5[a]	1900[b]
Glass	Amorphous	1.5[c]	1260[d]

[a]Reference 9.
[b]Reference 10.
[c]Reference 11.
[d]Reference 12.

layer completion, ℓ_3=3.9 Å. By inspection, the experimental slope $\Delta \simeq \frac{1}{2}$. The change in third-sound response at a coverage of $0.6\ell_3$ is attributed to the onset of first-excited-state occupation. For a discussion of possible models to describe the third-sound speed at higher coverages when the ^{3}He is also occupying the first excited state see Ref. 6.

The other third-sound experiment, by Valles, Heinrichs, and Hallock,[7] was on a borosilicate glass substrate. Data were taken for two values of the ^{4}He film thickness, 3.578 layers and 5.274 layers, where one ^{4}He layer ℓ_4=3.6 Å. We refer the reader to Ref. 7 and references cited therein for a discussion of the experimental details. These results qualitatively resemble the older thick-film results of Ref. 2: *little or no linear regime at low coverages*. If we assume that the very first few data points determine a line, then the slope is smaller for the thicker film and approximately $\Delta_{3.578} \simeq 0.8$ and $\Delta_{5.274} \simeq 0.6$.

There is at least one other mixture third-sound experiment in the literature. Noiray *et al.*[8] reported results for third sound on both Nuclepore and glass. These authors found a transition (they called a *stratification transition*) as a function of ^{4}He film thickness in which the ^{3}He was separated from the ^{4}He for large film thicknesses and mixes into the film at small film thickness. We shall investigate this behavior by calculating the ^{3}He density profile as a function of ^{4}He coverage.

The main purpose of this work is to investigate the low-^{3}He-coverage, layered-^{4}He-film, third-sound response on the Nuclepore and glass substrates and to try to understand why they are so different. Clearly, the essential physical difference between the Nuclepore/He and glass/He systems is the substrate-He potential. Different substrate potentials give rise to different ^{4}He and ^{3}He distributions. In Table I, we briefly compare Nuclepore and glass as substrates for ^{4}He. Both substrates are amorphous with no long-range periodic order. The van der Waals constant for glass is approximately 2/3 that of Nuclepore and the initial, immobile layer for glass is 5.4 Å thick compared to 9 Å for Nuclepore. Thus, the Nuclepore substrate is considerably more attractive than the glass.

In the following section, we begin a microscopic investigation of the two systems using the variational, hypernetted chain theory. The object will be to study the ^{3}He single-particle state and the various chemical potentials to obtain a better understanding of the underlying reason for the difference in the third-sound response of the Nuclepore and glass systems. In order to understand the physics we need to go beyond film-averaged hydrodynamics and examine the energies and distribution functions from a microscopic point of view. In Sec. II, we briefly review the microscopic hypernetted-chain–Euler-Lagrange (HNC-EL) theory. In Sec. III, we discuss the results of the microscopic calculations for the Nuclepore and glass model substrates. These are the first microscopic calculations of third-sound speeds for Nuclepore and glass substrates. Further, the results for the change in third-sound speed due to the addition of a small amount of ^{3}He represents the first microscopic calculation of the third-sound speed in a ^{3}He-^{4}He mixture film. Section IV is the Conclusion.

II. VARIATIONAL THEORY

In this section, we shall very briefly review the hypernetted chain Euler-Lagrange (HNC-EL) theory for helium films with single-particle physisorption states. The discussion emphasizes the calculation of the ^{4}He and ^{3}He chemical potentials. This discussion is necessary because the ^{4}He third-sound speed requires a density derivative of the chemical potential and the effect of the ^{3}He component on the third-sound speed requires a double-density derivative, and thus the numerical foundation of our results lies in the argument that the coverage dependence of the chemical potentials can be accurately determined. Details and further references of the general variational approach can be found in the review article in Ref. 13. In the first subsection, we first write down the equations needed to describe the ^{4}He film in a planar geometry. In the second subsection, we introduce a ^{3}He adatom and calculate the physisorption single-particle states and chemical potential.

A. ^{4}He films

The system consists of N ^{4}He atoms adsorbed to a solid substrate. The substrate-helium interaction is modeled by an appropriate external field $U_{\rm ext}(\mathbf{r}_i)$. The helium is described by a Feenberg variational wave function

$$\Psi_N(\mathbf{r}_1, \ldots, \mathbf{r}_N) = \exp \frac{1}{2}\left[\sum_i u_1^{(4)}(\mathbf{r}_i) + \sum_{i<j} u_2^{(4,4)}(\mathbf{r}_i, \mathbf{r}_j) + \sum_{i<j<k} u_3^{(4,4,4)}(\mathbf{r}_i, \mathbf{r}_j, \mathbf{r}_k) \right], \quad (2.1)$$

which allows for the breaking of translational invariance and isotropy as demanded by the external field. The ground state of the system is determined by functionally minimizing the expectation value of the N-body Hamiltonian

$$H_N = \sum_{i=1}^{N} \left[-\frac{\hbar^2}{2m}\nabla_i^2 + U_{\rm ext}(\mathbf{r}_i) \right] + \sum_{i<j} V(|\mathbf{r}_i - \mathbf{r}_j|) \quad (2.2)$$

in the space of all trial functions permitted in the ansatz (2.1).

For the pure ^{4}He film treated in this subsection, the superscripts on the variational functions u_n are superfluous. However, in the following subsection, when we add a ^{3}He atom to

the system, we need to explicitly include the flexibility of allowing the ^{3}He-^{4}He and ^{3}He-substrate correlations to be different from the ^{4}He-^{4}He and ^{4}He-substrate correlations. Having made this point, in the remainder of this subsection, we shall generally omit the "4" superscripts and subscripts for the sake of clarity.

The first task is to manipulate the expectation value of the Hamiltonian in a way that makes it accessible to numerical treatment. Symmetry breaking requires nontrivial one-body correlations as embodied in $u_1(\mathbf{r}_1)$. Our strategy will be to replace the functions u_n that are introduced in the many-body wave function, Eq. (2.1), by the physically observable n-body densities or distribution functions. The n-body density is defined as

$$\rho_n(\mathbf{r}_1, \ldots, \mathbf{r}_n) = \frac{N!}{(N-n)!}\frac{1}{I}\int d^3r_{n+1} \ldots d^3r_N \Psi_N^2(\mathbf{r}_1, \ldots, \mathbf{r}_N), \tag{2.3}$$

where I is the normalization integral

$$I = \int d^3r_1 \cdots d^3r_N \Psi_N^2(\mathbf{r}_1, \ldots, \mathbf{r}_N). \tag{2.4}$$

By calculating $\nabla_1\rho_4(\mathbf{r}_1)$ using the Feenberg wave function in Eq. (2.3) one obtains the first equation in the Born-Green-Yvon (BGY) hierarchy,

$$\nabla_1\rho_4(\mathbf{r}_1) = \rho_4(\mathbf{r}_1)\nabla_1 u_1(\mathbf{r}_1) + \rho_4(\mathbf{r}_1)\int d^3r_2 \rho_4(\mathbf{r}_2) g(\mathbf{r}_1,\mathbf{r}_2)\nabla_1 u_2(\mathbf{r}_1,\mathbf{r}_2), \tag{2.5}$$

where in an obvious notation $\rho_4(\mathbf{r})$ is the ^{4}He film profile. Equation (2.5) is exact for a wave function containing pair correlations only; a third term is added to the right-hand side if triplet correlations u_3 are included. We note that we shall use the symbol ρ [as in $\rho_4(\mathbf{r})$] to denote volume number densities and the symbol σ to denote areal number densities (i.e., the coverage).

Equation (2.5) is be used to eliminate $u_1(\mathbf{r})$. For the pair function $u_2(\mathbf{r}_1,\mathbf{r}_2)$, we use the HNC hierarchy of integral equations for inhomogeneous systems to derive a relationship between $u_2(\mathbf{r}_1,\mathbf{r}_2)$ and the pair distribution function $g(\mathbf{r}_1,\mathbf{r}_2)$. The cleanest, but somewhat lengthy diagrammatic derivation of the HNC equations for a nonuniform system may be found in Ref. 14; a somewhat heuristic derivation, tuned to the application to quantum liquids, was given in Ref. 15.

The HNC equations are

$$g(\mathbf{r}_1,\mathbf{r}_2) = \exp[u_2(\mathbf{r}_1,\mathbf{r}_2) + N(\mathbf{r}_1,\mathbf{r}_2) + E(\mathbf{r}_1,\mathbf{r}_2)], \tag{2.6}$$

$$\tilde{N}(\mathbf{r}_1,\mathbf{r}_2) = [\tilde{h} * \tilde{X}](\mathbf{r}_1,\mathbf{r}_2), \tag{2.7}$$

$$h(\mathbf{r}_1,\mathbf{r}_2) = g(\mathbf{r}_1,\mathbf{r}_2) - 1, \tag{2.8}$$

$$X(\mathbf{r}_1,\mathbf{r}_2) = h(\mathbf{r}_1,\mathbf{r}_2) - N(\mathbf{r}_1,\mathbf{r}_2), \tag{2.9}$$

where $N(\mathbf{r}_1,\mathbf{r}_2)$ are the chain (nodal) diagrams and $X(\mathbf{r}_1,\mathbf{r}_2)$ are the non-nodal diagrams. Here $E(\mathbf{r}_1,\mathbf{r}_2)$ is the infinite series of "elementary" diagrams which can be expressed as multidimensional integrals involving $\rho_4(\mathbf{r})$ and $g(\mathbf{r}_1,\mathbf{r}_2)$. It may also contain triplet correlations.

Square roots of the density appear frequently as factors. In Eq. (2.7) and henceforth, we introduce the "tilde notation"—for example,

$$\tilde{C}(\mathbf{r}_1) \equiv \sqrt{\rho_4(\mathbf{r}_1)}C(\mathbf{r}_1), \tag{2.10}$$

$$\tilde{A}(\mathbf{r}_1,\mathbf{r}_2) \equiv \sqrt{\rho_4(\mathbf{r}_1)}A(\mathbf{r}_1,\mathbf{r}_2)\sqrt{\rho_4(\mathbf{r}_2)}. \tag{2.11}$$

We also mark convolution products with an asterisk. The unit operator and the inverse will generally be interpreted in the sense of a convolution product. We shall also use the coordinate-space static structure function

$$S(\mathbf{r},\mathbf{r}') = \delta(\mathbf{r},\mathbf{r}') + \tilde{h}(\mathbf{r},\mathbf{r}'), \tag{2.12}$$

which is related to the direct correlation function $X(\mathbf{r}_1,\mathbf{r}_2)$ through

$$S(\mathbf{r}_1,\mathbf{r}_2) = [\mathbf{1} - \tilde{X}]^{-1}(\mathbf{r}_1,\mathbf{r}_2). \tag{2.13}$$

The variational energy expectation value is given by

$$E_N[u_n] = \frac{1}{I}\int d^3r_1 \cdots d^3r_N \Psi_N(\mathbf{r}_1, \ldots, \mathbf{r}_N) H \Psi_N(\mathbf{r}_1, \ldots, \mathbf{r}_N). \tag{2.14}$$

If triplet correlations are neglected for the time being, one can, using the HNC relationship (2.6), express E_N entirely in terms of the one-body density $\rho_4(\mathbf{r}_1)$ and the pair distribution function and $g(\mathbf{r}_1,\mathbf{r}_2)$,

$$E_N = T^{(4)} + E_{\mathrm{ext}}^{(4)} + E_c, \tag{2.15}$$

$$E_c = K + V + E_Q, \tag{2.16}$$

$$K = \frac{\hbar^2}{2m}\int d^3r_1 d^3r_2 \rho_4(\mathbf{r}_1)\rho_4(\mathbf{r}_2)[|\nabla_1\sqrt{g(\mathbf{r}_1,\mathbf{r}_2)}|^2 + |\nabla_2\sqrt{g(\mathbf{r}_1,\mathbf{r}_2)}|^2], \tag{2.17}$$

$$V = \frac{1}{2}\int d^3r_1 d^3r_2 \rho_4(\mathbf{r}_1)\rho_4(\mathbf{r}_2) g(\mathbf{r}_1,\mathbf{r}_2) V(|\mathbf{r}_1 - \mathbf{r}_2|), \tag{2.18}$$

$$E_Q = -\frac{1}{4}\int d^3r_1 d^3r_2 [\tilde{N}(\mathbf{r}_1,\mathbf{r}_2) + \tilde{E}(\mathbf{r}_1,\mathbf{r}_2)] H_1(\mathbf{r}_1)\tilde{h}(\mathbf{r}_1,\mathbf{r}_2), \tag{2.19}$$

where

$$H_1(\mathbf{r}_1) = -\frac{\hbar^2}{2m}\frac{1}{\sqrt{\rho_4(\mathbf{r}_1)}}\boldsymbol{\nabla}_1\cdot\rho_4(\mathbf{r}_1)\boldsymbol{\nabla}_1\frac{1}{\sqrt{\rho_4(\mathbf{r}_1)}}. \quad (2.20)$$

The operator $H_1(\mathbf{r}_1)$ can be thought of as the kinetic energy operator generalized to inhomogeneous systems.

Two new quantities appear in Eq. (2.15). The first one

$$T^{(4)} = \frac{\hbar^2}{2m}\int d^3r_1|\boldsymbol{\nabla}_1\sqrt{\rho_4(\mathbf{r}_1)}|^2 \quad (2.21)$$

is the kinetic energy of a noninteracting, inhomogeneous Bose system whose single-particle wave function is $\sqrt{\rho_1(\mathbf{r}_1)}$. The second term

$$E_{\text{ext}}^{(4)} = \int d^3r_1\rho_4(\mathbf{r}_1)U_{\text{ext}}(\mathbf{r}_1) \quad (2.22)$$

is the energy of the system in the external field $U_{\text{ext}}(\mathbf{r}_1)$. This physics of the interactions is contained in the third term E_c, which we shall call the "correlation energy."

The functions $\rho_4(\mathbf{r}_1)$ and $g(\mathbf{r}_1,\mathbf{r}_2)$ are determined by minimization of the total energy. Let us first look at the optimization of the pair correlations. One arrives at the Euler-Lagrange equation[15]

$$[\tilde{X} * H_1 * \tilde{X}](\mathbf{r}_1,\mathbf{r}_2) - [H_1(\mathbf{r}_1) + H_1(\mathbf{r}_2)]\tilde{X}(\mathbf{r}_1,\mathbf{r}_2) = 2\tilde{V}_{\text{p-h}}^{(44)}(\mathbf{r}_1,\mathbf{r}_2) \quad (2.23)$$

or, using the relationship (2.13),

$$[S^{-1} * H_1 * S^{-1} - H_1](\mathbf{r}_1,\mathbf{r}_2) = 2\tilde{V}_{\text{p-h}}^{(44)}(\mathbf{r}_1,\mathbf{r}_2). \quad (2.24)$$

The "particle-hole interaction" $V_{\text{p-h}}^{(44)}(\mathbf{r}_1,\mathbf{r}_2)$ appearing in Eq. (2.23) is

$$V_{\text{p-h}}^{(44)}(\mathbf{r}_1,\mathbf{r}_2) = g(\mathbf{r}_1,\mathbf{r}_2)[V(|\mathbf{r}_1-\mathbf{r}_2|)] + \Delta V_e(\mathbf{r}_1,\mathbf{r}_2) + \frac{\hbar^2}{2m}[|\boldsymbol{\nabla}_1\sqrt{g(\mathbf{r}_1,\mathbf{r}_2)}|^2 + |\boldsymbol{\nabla}_2\sqrt{g(\mathbf{r}_1,\mathbf{r}_2)}|^2] + h(\mathbf{r}_1,\mathbf{r}_2)w_I(\mathbf{r}_1,\mathbf{r}_2), \quad (2.25)$$

with the induced interaction

$$\tilde{w}_I(\mathbf{r}_1,\mathbf{r}_2) = -\frac{1}{2}[[H_1(\mathbf{r}_1) + H_1(\mathbf{r}_2)]\tilde{N}(\mathbf{r}_1,\mathbf{r}_2) + [\tilde{X} * H_1 * \tilde{X}](\mathbf{r}_1,\mathbf{r}_2)]. \quad (2.26)$$

$\Delta V_e(\mathbf{r}_1,\mathbf{r}_2)$ denotes the correction from elementary diagrams and triplet correlations. The nomenclature "particle-hole interaction" is used because in an exact theory this term would be equal to the second functional derivative of the energy with respect to the density. It is important to understand at this point that the HNC expression (2.25) is identical with the second density derivative only in an exact theory that contains all elementary diagrams and multiparticle correlations to all orders. Turning the discrepancy to an advantage, the comparison between the HNC definition and the second functional derivative can serve as a useful consistency test. By a cautious scaling of triplet and elementary diagram corrections, these quantities may also be made equal; it is our experience that such modifications have no visible effect on quantities like the energy or density profiles, and they can slightly alter the stability limits.

Finally, we must also derive an Euler equation for the one-body density. The energy is minimized subject to the constraint of fixed particle number

$$N = \int d^3r_1\rho_4(\mathbf{r}_1); \quad (2.27)$$

i.e., we carry out the variation

$$\frac{1}{2}\frac{\delta(E_N-\mu_4N)}{\delta\sqrt{\rho_4(\mathbf{r}_1)}} = \left[-\frac{\hbar^2}{2m}4\boldsymbol{\nabla}_1^2 + U_{\text{ext}}(\mathbf{r}_1) + V_{\text{H}}^{(4)}(\mathbf{r}_1) - \mu_4\right]\times\sqrt{\rho_4(\mathbf{r}_1)} = 0, \quad (2.28)$$

where

$$V_{\text{H}}^{(4)}(\mathbf{r}_1) = \frac{\delta E_c}{\delta\rho_4(\mathbf{r}_1)} \quad (2.29)$$

is a generalized Hartree potential that depends implicitly on the density and the pair distribution function. The chemical potential μ_4 enters the theory as a Lagrange parameter to enforce the constraint (2.27). Explicit forms of the effective one-body potential $V_H(\mathbf{r})$ have been derived in Ref. 16.

The central quantities of interest in this work are the ^{3}He and ^{4}He coverage dependences of the third-sound speed, c_3. The third-sound speed can be calculated in two different ways: namely, as the hydrodynamic derivative

$$m_4c_3^2 = \sigma_4\frac{d\mu_4(\sigma_4)}{d\sigma_4} \quad (2.30)$$

and from the long-wavelength limit of the low-lying excitations.

Taking the derivative of the ρ_4 equation (2.28) with respect to σ_4 yields

$$\left[-\frac{\hbar^2}{2m}4\boldsymbol{\nabla}^2 + U_{\text{ext}}(\mathbf{r}) + V_{\text{H}}^{(4)}(\mathbf{r}) - \mu_4\right]\frac{d\sqrt{\rho_4(\mathbf{r})}}{d\sigma_4} + \frac{dV_{\text{H}}^{(4)}(\mathbf{r})}{d\sigma_4}\sqrt{\rho_4(\mathbf{r})} = \frac{d\mu_4}{d\sigma_4}\sqrt{\rho_4(\mathbf{r})}. \quad (2.31)$$

The density derivatives of the Hartree potentials can be rewritten in terms of the *particle-hole interaction* $V_{\text{p-h}}^{(44)}(\mathbf{r},\mathbf{r}')$,

$$V_{\text{p-h}}^{(ij)}(\mathbf{r},\mathbf{r}') = \frac{\delta^2E_{\text{c}}}{\delta\rho_i(\mathbf{r})\delta\rho_j(\mathbf{r}')}, \quad (2.32)$$

where $i,j=3,4$, as

$$\frac{dV_{\text{H}}^{(4)}(\mathbf{r})}{d\sigma_4} = \int d^3r'\frac{\delta V_{\text{H}}^{(4)}(\mathbf{r})}{\delta\rho_4(\mathbf{r}')}\frac{d\rho_4(\mathbf{r}')}{d\sigma_4} = \int d^3r'V_{\text{p-h}}^{(44)}(\mathbf{r},\mathbf{r}')\frac{d\rho_4(\mathbf{r}')}{d\sigma_4}. \quad (2.33)$$

The HNC form of Eq. (2.32) was introduced in Eq. (2.25).

The operator on the left-hand side of Eq. (2.31) can be rewritten as follows:

$$\left[-\frac{\hbar^2}{2m}{}_i\nabla^2 + U_{\rm ext}(\mathbf{r}) + V_{\rm H}^{(i)}(\mathbf{r}) - \mu_i\right]$$
$$= -\frac{\hbar^2}{2m}{}_i\frac{1}{\sqrt{\rho_i(\mathbf{r})}}\nabla\rho_i(\mathbf{r})\cdot\nabla\frac{1}{\sqrt{\rho_i(\mathbf{r})}}$$
$$= -\frac{\hbar^2}{2m}{}_i\left[\nabla^2 - \frac{\nabla^2\sqrt{\rho_i(\mathbf{r})}}{\sqrt{\rho_i(\mathbf{r})}}\right]$$
$$\equiv H_1^{(i)}(\mathbf{r}). \tag{2.34}$$

The density derivative equation (2.31) can thus be written as an integral equation

$$\int d^3r'[H_1^{(4)}(\mathbf{r})\delta(\mathbf{r}-\mathbf{r}') + 2\tilde{V}_{\text{p-h}}^{(44)}(\mathbf{r},\mathbf{r}')]\frac{d\sqrt{\rho_4(\mathbf{r}')}}{d\sigma_4}$$
$$= \frac{d\mu_4}{d\sigma_4}\sqrt{\rho_4(\mathbf{r})}. \tag{2.35}$$

Formally inverting the operator in square brackets and then multiplying by $\sqrt{\rho_4(\mathbf{r})}$ and integrating over $\mathbf{r}$ finally leads to

$$\sigma_4\frac{d\mu_4(\sigma_4)}{d\sigma_4} = \frac{1}{2}\frac{\sigma_4}{(\sqrt{\rho_4}|[H_1^{(4)} + 2\tilde{V}_{\text{p-h}}^{(44)}]^{-1}|\sqrt{\rho_4})}, \tag{2.36}$$

in an obvious notation.

An alternative derivation is to look at the long-wavelength limit of the low-lying excitation, which is, in our case, third sound. One then arrives[15] at exactly the same expression (2.36); however, in that case the particle-hole interaction $V_{\text{p-h}}^{(44)}$ is given by the HNC expression (2.25). Thus, comparing the speed of third sound as obtained from the density derivative of the chemical potential with the one obtained from long-wavelength excitations gives some estimate for the accuracy of the HNC approximation for $V_{\text{p-h}}^{(44)}$.

B. ^{3}He single-particle states

The Hamiltonian of the $(N+1)$-particle system consisting of N ^{4}He atoms and one ^{3}He is

$$H_{N+1} = -\frac{\hbar^2}{2m_3}\nabla_0^2 + U_{\rm ext}(\mathbf{r}_0) + \sum_{i=1}^{N} V(|\mathbf{r}_0 - \mathbf{r}_i|) + H_N. \tag{2.37}$$

We adopt the convention that the coordinate $\mathbf{r}_0$ refers to the ^{3}He particle and coordinates $\mathbf{r}_i$, with $i=1,\ldots,N$, to the ^{4}He film particles. The theory is easily generalizable to arbitrary impurity atoms by introducing specific functions for the impurity interaction with the substrate and the ^{4}He.

The generalization of the wave function (2.1) for an inhomogeneous N-particle ^{4}He system with a single ^{3}He atom is

$$\Psi_{N+1}(\mathbf{r}_0,\mathbf{r}_1,\ldots,\mathbf{r}_N)$$
$$= \exp\frac{1}{2}\left[u_1^{(3)}(\mathbf{r}_0) + \sum_{1\le i\le N} u_2^{(3,4)}(\mathbf{r}_0,\mathbf{r}_i) + \sum_{1\le i<j\le N} u_3^{(3,4,4)}(\mathbf{r}_0,\mathbf{r}_i,\mathbf{r}_j)\right]\Psi_N(\mathbf{r}_1,\ldots,\mathbf{r}_N). \tag{2.38}$$

The energy change due to adding one ^{3}He atom into the system is the ^{3}He chemical potential $\mu_3 \equiv E_{N+1} - E_N$, where E_{N+1} is the energy of the system containing one ^{3}He and N ^{4}He atoms and E_N is the energy of the unperturbed ^{4}He film, Eq. (2.15). Here E_{N+1} is to be understood as the energy expectation value of the Hamiltonian (2.37) with respect to the wave function (2.38).

We find that the ^{3}He chemical potential can be written in the form

$$\mu_3 = T^{(3)} + E_{\rm ext}^{(3)} + \Delta E_c. \tag{2.39}$$

The first term is the kinetic energy of a single noninteracting ^{3}He atom with ground-state wave function $\sqrt{\rho_3(\mathbf{r}_0)}$,

$$T^{(3)} = \frac{\hbar^2}{2m_3}\int d^3r_0|\nabla\sqrt{\rho_3(\mathbf{r}_0)}|^2, \tag{2.40}$$

and the second term is the energy of the ^{3}He in the external potential,

$$E_{\rm ext}^{(3)} = \int d^3r_0 U_{\rm ext}(\mathbf{r}_0)\rho_3(\mathbf{r}_0). \tag{2.41}$$

The correlation energy ΔE_c contains the many-body effects, which can be written as a functional of four quantities: the ^{3}He density $\rho_3(\mathbf{r}_0)$, the ^{4}He film density $\rho_4(\mathbf{r}_1)$, the ^{3}He-^{4}He pair-distribution function $g^{(34)}(\mathbf{r}_0,\mathbf{r}_1)$, and the ^{4}He pair-distribution function $g^{(44)}(\mathbf{r}_1,\mathbf{r}_2)$.

When minimizing the ^{3}He energy, one must keep in mind that all background quantities are changed by the presence of the ^{3}He atom by terms of the order of $1/N$; these changes give rise to quantitatively important rearrangement effects. The details of the derivation are given in Ref. 17, the final results being similar to those of the ground-state theory of the background film.

The ^{3}He density is calculated by minimizing the chemical potential (2.39) with respect to $\sqrt{\rho_3(\mathbf{r}_0)}$. This leads to the usual Hartree equation

$$-\frac{\hbar^2}{2m_I}\nabla_0^2\sqrt{\rho_3(\mathbf{r}_0)} + [U_{\rm ext}(\mathbf{r}_0) + V_H^{(3)}(\mathbf{r}_0)]\sqrt{\rho_3(\mathbf{r}_0)} = \mu_3\sqrt{\rho_3(\mathbf{r}_0)}, \tag{2.42}$$

with the self-consistent one-body Hartree potential for the single ^{3}He atom:

$$V_{\rm H}^{(3)}(\mathbf{r}_0) = \frac{\delta\Delta E_c}{\delta\rho_3(\mathbf{r}_0)}. \tag{2.43}$$

The ^{3}He chemical potential μ_3 appears as the Lagrange multiplier to ensure the normalization $\int d^3r_0\rho_3(\mathbf{r}_0) = 1$. The two-body Euler equation is derived by variation of the ^{3}He chemical potential with respect to $\sqrt{g^{(34)}(\mathbf{r}_0,\mathbf{r}_3}$. One obtains a result that is similar to Eq. (2.23) above and the solution proceeds analogously.

In a manner similar to the derivation of the third-sound speed, we can calculate the σ_4 derivative of μ_3:

$$\left[-\frac{\hbar^2}{2m_3}\nabla^2 + U_{\rm ext}(\mathbf{r}) + V_{\rm H}^{(3)}(\mathbf{r}) - \mu_3\right]\frac{d\sqrt{\rho_3(\mathbf{r})}}{d\sigma_4} + \frac{dV_{\rm H}^{(3)}(\mathbf{r})}{d\sigma_4}\sqrt{\rho_3(\mathbf{r})} = \frac{d\mu_3}{d\sigma_4}\sqrt{\rho_3(\mathbf{r})}. \tag{2.44}$$

Multiplying Eq. (2.44) by $\sqrt{\rho_3(\mathbf{r})}$ and integrating over $\mathbf{r}$, we find:

$$\sigma_3\frac{d\mu_3}{d\sigma_4} = \int d^3r\rho_3(\mathbf{r})\frac{dV_{\rm H}^{(3)}(\mathbf{r})}{d\sigma_4} = 2\int d^3r d^3r'\sqrt{\rho_3(\mathbf{r})}\tilde{V}_{\text{p-h}}^{(34)}(\mathbf{r},\mathbf{r}')\frac{d\sqrt{\rho_4(\mathbf{r}')}}{d\sigma_4}, \tag{2.45}$$

which is the desired relationship.

C. ^{3}He dynamics

The "Hartree equation" (2.42) can readily be interpreted to provide a first level of approximation for the excited states of the ^{3}He atom,

$$-\frac{\hbar^2}{2m_3}\nabla^2\eta_i(\mathbf{r}_0) + [U_{\rm ext}(\mathbf{r}_0) + V_{\rm H}^{(3)}(\mathbf{r}_0) - \mu_3]\eta_i(\mathbf{r}_0) = t_i\eta_i(\mathbf{r}_0), \tag{2.46}$$

where, for the ground state, $t_0=0$ and $\eta_0(\mathbf{r}_0)=\sqrt{\rho_3(\mathbf{r}_0)}$. The interpretation of the eigenvalue-function pairs $\{t_i, \eta_i(\mathbf{r}_0)\}$ as excited states leaves out a number of effects.

(i) If the momentum is a good quantum number, low-lying excited states can be characterized in terms of an *effective mass*. In our geometry, an effective mass is associated with the motion of an ^{3}He particle *parallel* to the surface. This "hydrodynamic" effective mass is caused by the coupling of the ^{3}He motion to the excitations of the background liquid. At the $\{t_i, \eta_i(\mathbf{r}_0)\}$ level, the effective mass is the bare mass.

(ii) The effective Hartree potential $V_H^{(3)}(z)$ is real. Thus, at the $\{t_i, \eta_i(\mathbf{r}_0)\}$ level, the "excitations" defined by the local equation (2.42) have an infinite lifetime. This is also a consequence of the static approximation.

In order to treat these effects more properly, a generalization of the stationary correlation picture of Eq. (2.38) that leads Eq. (2.46) is needed. A proper theory should describe resonances and allow for their decay by the coupling to the low-lying background excitations of the host film.

The natural generalization of the variational approach to excited states is to allow for a time dependence of the variational functions $u_n(\mathbf{r}_0,\ldots,\mathbf{r}_n;t)$. We outline here only the basic steps; the reader is referred to Ref. 17 for details. We begin by separating the *kinematic* from the *dynamic* correlations and write the time-dependent variational wave function in the form

$$\phi(t) = \frac{1}{\sqrt{\langle\psi_{N+1}|\psi_{N+1}\rangle}}e^{-iE_{N+1}t/\hbar}\psi_{N+1}(\mathbf{r}_0,\mathbf{r}_1,\ldots,\mathbf{r}_N;t), \tag{2.47}$$

where $\psi_{N+1}(\mathbf{r}_0,\mathbf{r}_1,\ldots,\mathbf{r}_N;t)$ contains the dynamic, time-dependent correlations. Consistent with the general strategy of variational methods, we include the time dependence in the one-particle *and* two-particle ^{3}He-background correlations; i.e., we write

$$\psi_{N+1}(\mathbf{r}_0,\mathbf{r}_1,\ldots,\mathbf{r}_N;t) = \exp\frac{1}{2}\left[\delta u_1(\mathbf{r}_0;t) + \sum_{1\leqslant i\leqslant N}\delta u_2(\mathbf{r}_0,\mathbf{r}_i;t)\right]\times\Psi_{N+1}(\mathbf{r}_0,\mathbf{r}_1,\ldots,\mathbf{r}_N). \tag{2.48}$$

The time independent part remains the same as defined in Eq. (2.38). The time-dependent correlations are determined by searching for a stationary state of the action integral

$$\mathcal{S} = \int_{t_0}^{t}\mathcal{L}(t)dt,$$

$$\mathcal{L}(t) = \langle\phi(t)|\left(H_{N+1} - i\hbar\frac{\partial}{\partial t}\right)|\phi(t)\rangle, \tag{2.49}$$

where H_{N+1} is the Hamiltonian (2.37) of the ^{3}He plus ^{4}He-film system.

It is convenient to work in the basis defined by the ^{3}He states $\eta_i(\mathbf{r}_0)$. We expand the time dependent part of the single-particle density

$$\delta\rho_3(\mathbf{r}_0;t) = \langle\phi(t)|\hat{\rho}_3(\mathbf{r})|\phi(t)\rangle, \tag{2.50}$$

where $\hat{\rho}_3(\mathbf{r})$ is the one-body density operator, in terms of the single-particle states $\eta_i(\mathbf{r}_0)$:

$$\frac{\delta\rho_3(\mathbf{r};t)}{\sqrt{\rho_3(\mathbf{r})}} = e^{-i\omega t}\sum_i r_i\eta_i(\mathbf{r}). \tag{2.51}$$

The equation of motion for the amplitudes r_p has been derived in Ref. 17; it takes the form of an energy-dependent one-body equation

$$\hbar\omega r_i = \sum_j[\delta_{ij}t_i + \Sigma_{ij}(\omega)]r_j, \tag{2.52}$$

where

$$\Sigma_{ij}(\omega) = -\sum_{mk}\frac{W_{mk}^{*(i)}W_{mk}^{(j)}}{\hbar\omega_m + t_k - \hbar\omega} \tag{2.53}$$

is to be interpreted as the ^{3}He self-energy. The $\hbar\omega_m$ are the collective excitations of the background liquid. The ^{3}He-^{3}He-ripplon vertex function $W_{mq}^{(p)}$ occurring in the self-energy (2.53) has the form of an effective interaction within the theory of correlated basis functions,[18–20] its specific form being irrelevant for our further discussions. We only need to mention the important fact that Eq. (2.52) does not renormalize the ^{3}He ground state.

Two simple applications of this approach are the calculation of the hydrodynamic effective mass of the ^{3}He and the calculation of the excited-state energy. For the ground state and small parallel momenta, we can expand

$$\hbar\omega(q_\parallel) = \frac{\hbar^2 q_\parallel^2}{2m} + \frac{1}{2}q_\parallel^2 \left.\frac{d^2\Sigma_{0,0}(q_\parallel)}{dq_\parallel^2}\right|_{q_\parallel=0} \equiv \frac{\hbar^2 q_\parallel^2}{2m^*} \quad (2.54)$$

and obtain an effective mass.

To get excited states at zero parallel momentum, one must solve Eq. (2.52) self-consistently. For higher-lying excitations, the phase-space integrals of Eq. (2.53) have a pole and must be interpreted as principal value integrals; i.e., they are complex. Therefore, all excited states acquire a finite lifetime, as they should, by being able to decay into the ground state through the emission of ripplons or phonons. Hence, dynamic correlations define both the effective mass and, via the same mechanism, the lifetime of the ^{3}He physisorption states.

III. RESULTS

A. Energetics

In the small-^{3}He-concentration regime, we can write

$$\mu_4(N_3,N_4) \simeq \mu_{40} + \left(\frac{\partial\mu_4}{\partial\sigma_3}\right)_0 \sigma_3. \quad (3.1)$$

We can use this to obtain a third-sound speed, in terms of the incompressibility ($\equiv mc^2$), in the small-^{3}He-concentration limit. By taking the derivative with respect to σ_4,

$$m_4 c_3^2 = m_4 c_{30}^2 + \sigma_4\sigma_{3\ell}\left[\frac{\partial}{\partial\sigma_4}\left(\frac{\partial\mu_4}{\partial\sigma_3}\right)_0\right]\theta_3, \quad (3.2)$$

where θ_3 is the coverage in units of layers as defined below Eq. (1.3). If we put this in the form of the hydrodynamic equations, Eq. (1.3), we immediately find the "thermodynamic" slope given by

$$\Delta_{\text{thermo}} = -\frac{\sigma_4\sigma_{3\ell}}{m_4 c_{30}^2}\frac{\partial}{\partial\sigma_4}\left(\frac{\partial\mu_4}{\partial\sigma_3}\right)_0. \quad (3.3)$$

We remind the reader that σ_3, σ_4, and $\sigma_{3\ell}$ are *areal* number densities. In the following, we shall report results in terms of Eq. (3.2) instead of Eq. (3.3) because, as shown below, a first-principles theory yields regions in which the pure ^{4}He third-sound speed vanishes. We can avoid a full mixture calculation with variable population of ^{3}He for calculating the derivative in Eq. (3.2) by taking advantage of the Maxwell relation

$$\left(\frac{\partial\mu_4}{\partial\sigma_3}\right)_{\mathcal{A},T,N_4} = \left(\frac{\partial\mu_3}{\partial\sigma_4}\right)_{\mathcal{A},T,N_3}. \quad (3.4)$$

Equation (3.4) is derived in the Appendix from thermodynamic arguments. We also explicitly obtain microscopic equations for the density derivatives. The starting points for the microscopic analysis are Eqs. (2.28) and (2.42) for the ^{4}He and ^{3}He chemical potentials, respectively. Using these chemical potentials in Eq. (3.3) we can examine the experimental third-sound results using microscopic theory and compare with the film-averaged hydrodynamic models. We shall discuss the pure ^{4}He third-sound speed as a function of film thickness for both substrates. In addition, we shall use Eq. (3.2) to examine the effect of ^{3}He on the third-sound speed in the low-^{3}He-coverage limit.

One expects that film-averaged, hydrodynamic models should give the right answer in the limit of thick ^{4}He films where any surface-normal structure can be averaged out. This will not be the case for *thin* ^{4}He films on strongly interacting substrates where it is clearly understood that the ^{4}He atom arranges itself in a layered structure.[13,21] That is, in the thick-film limit, the correlation contribution to the chemical potential of an added ^{4}He atom is basically a constant and any change in the chemical potential is due solely to the external field. For a layered system the change in the chemical potential has important contributions from the correlations in addition to that of the external field.

In this work we have studied the two substrates Nuclepore and glass characterized in Table I. An important word is necessary as to how we have dealt with the immobile layers. In the case of Nuclepore, we assumed two solid layers at a distance from the substrate of 3.6 Å and 7.2 Å. The areal densities of the layers are $\sigma_1 = 0.11$ Å^{-2} and $\sigma_2 = 0.09$ Å^{-2}, respectively, adding the amount of ^{4}He corresponding to roughly 2.5 *liquid* layers. For the glass substrate, we assumed one immobile layer of areal density $\sigma_1 = 0.11$ Å^{-2}, corresponding to roughly 1.5 liquid layers. We consider these atoms as rigid and obtain a correction to the substrate potentials of Table I by averaging Lennard-Jones potentials over two or one planes, respectively. When the short-ranged part of the substrate potential is screened in such a way, the results basically depend only on the long-ranged part.

We first examine the key energetic quantities: the ^{3}He and ^{4}He chemical potentials and the ^{3}He first excited state as functions of ^{4}He film coverage. These are shown, for the Nuclepore and glass substrates, in Figs. 1 and 2, respectively. In these figures, we also show a fit to the numerical data of the form

$$\mu_4(\sigma) = \mu_4(\infty) - \frac{\alpha_s\bar{\rho}^3}{\sigma^3} + \frac{c}{\sigma^4} + \frac{d}{\sigma^5} + \frac{e\cos(k\sigma-\gamma)}{\sigma^4}. \quad (3.5)$$

The second term on the right-hand side is the usual van der Waals expression, and the last three terms are empirical.

Both films undergo several layering transitions. The strongest is at second-layer formation. For the Nuclepore substrate, Fig. 1, this transition occurs in the regime 0.070 Å^{-2} $\leqslant\sigma_4\leqslant$ 0.10 Å^{-2}. For the glass substrate, Fig. 2, this transition occurs in the regime 0.075 Å$^{-2}\leqslant\sigma_4\leqslant$0.105 Å^{-2}. No translationally invariant film configurations exist in these regimes. The numerical fits for Eq. (3.5) were therefore carried out only in the coverage regime of two and more layers, $\sigma_4 > 0.10$ Å^{-2}. From the fit, we can read off the bulk limit of the chemical potential, which comes out to be −7.30 K for the case of glass and −7.36 K in the case of Nuclepore, in good agreement with the experimental value.

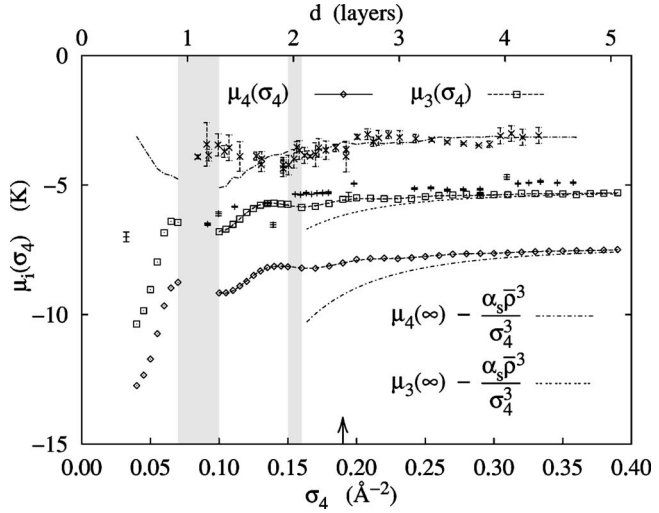

FIG. 1. For the Nuclepore substrate, the calculated ^{4}He chemical potential (diamonds), the ^{3}He chemical potential (boxes), and the ^{3}He first-excited-state energies (dash-dotted line). Also shown are the full fits (3.5) to the ^{4}He (solid line) and the ^{3}He (dashed line) chemical potentials, as well as the asymptotic forms (3.6) (short-dashed and long-short-dashed lines). The gray areas are inaccessible regimes of layering transitions. The symbols shown on the first-excited-state line ($\times$'s) are the experimental measurements as reported by Sprague *et al.* (Ref. 22). The arrow located at 0.19 Å^{-2} is our best estimate for the mobile film coverage corresponding to the experiment of Sheldon and Hallock (Ref. 5). The upper scale gives the thickness of the films in *liquid* layers; one ^{4}He layer is defined as representing an areal density of 0.077 Å^{-2}.

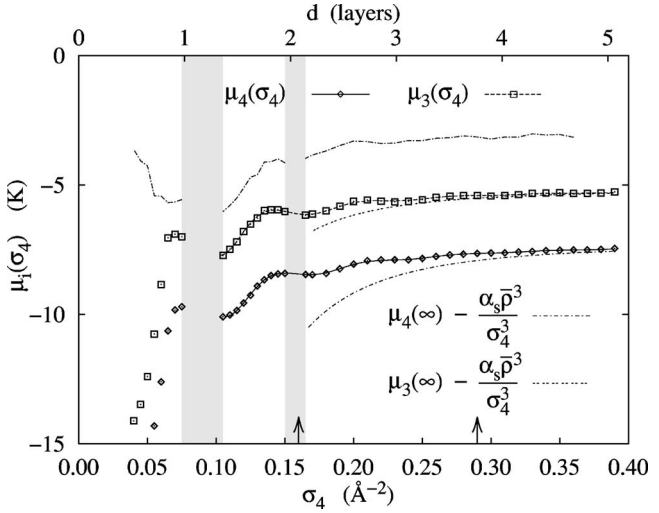

FIG. 2. For the glass substrate, the calculated ^{4}He chemical potential (diamonds), the ^{3}He chemical potential (boxes), and the ^{3}He first-excited-state-energies (dash-dotted line). Also shown are the full fits (3.5) to the ^{4}He (solid line) and the ^{3}He (dashed line) chemical potentials, as well as the asymptotic forms (3.6) (short-dashed and long-short-dashed lines). The gray areas are inaccessible regimes of layering transitions. The arrows located at 0.16 and 0.29 Å^{-2} are our best estimates for the mobile film coverage corresponding to the experiment of Valles, Heinrichs, and Hallock (Ref. 7). The upper scale gives the thickness of the films in *liquid* layers; one ^{4}He layer is defined as representing an areal density of 0.077 Å^{-2}.

The term proportional to σ^{-3} contains the van der Waals constant α_s and an average density $\bar{\rho}$. If the value of α_s is fixed (see Table I), then we find that the quality of the fit for $\bar{\rho}$ is unchanged for 0.020 Å$^{-3} \leqslant \bar{\rho} \leqslant 0.022$ Å^{-3}. This result is consistent with both the experimental bulk equilibrium density and the fact that our treatment of elementary diagrams and triplet correlations leads to a calculated equilibrium density that is slightly lower than experiment. The oscillatory term in Eq. (3.5) reflects a periodic, layered structure, its "wavelength" of 0.066 Å^{-2} being practically identical in all cases.

The most dramatic information in Figs. 1 and 2 concerns the comparison between the microscopic chemical potentials and the van der Waals limit

$$\lim_{\sigma\to\infty} \mu_i(\sigma) \sim \mu_i(\infty) - \frac{\alpha_s\bar{\rho}^3}{\sigma^3}, \tag{3.6}$$

for $i=3,4$. *For thin films on Nuclepore or glass, there is no region in which the van der Waals form is in agreement with the calculated, microscopic chemical potentials.* In the regime $d \gtrsim 3$ layers, the agreement between the microscopic and van der Waals form is simply a statement that the bulk quantities $\mu_i(\infty)$ are being fit correctly. We note in particular that the function $\mu_4(\sigma)$, in the coverage regime 0.2 Å^{-2} $\leqslant \sigma_4 \leqslant$ 0.2 Å^{-2}, is much flatter than what the asymptotic form (3.6) suggests. This explains the uncertainty in determining $\bar{\rho}$ from the fit to the chemical potential.

It is important to emphasize that when translating the immobile layer thickness from Table I into a coverage a small amount of uncertainty is introduced in the coverage scale of Figs. 1 and 2 and also the two following figures. In these figures, zero coverage begins at the beginning of the *mobile* film. In order to make contact with experiment, we need to subtract the immobile film coverage from the total film coverage as reported for the experiments. The coverage of the immobile film, as explained above, is unknown and must be inferred. For example, in Fig. 1, the arrow ostensibly locating the coverage corresponding to the experiment of Sheldon and Hallock[5] is positioned at 0.19 Å^{-2}; this represents the difference between the reported total film coverage of 0.389 Å^{-2} and our best estimate for the immobile film coverage, 0.2 Å^{-2}.

In order to gauge the accuracy of our calculations we need to compare our results with experiment. In a series of papers, Hallock and co-workers[22–24] reported measurements of the ^{3}He ground-state and first-excited-state energies in the low-^{3}He-concentration limit as a function of ^{4}He coverage on Nuclepore. In Figs. 1 and 2, we report the energies of the ^{3}He first excited state, calculated within the dynamic theory of Sec. II C, for both substrates. In Fig. 1, shown as $\times$'s, we overlay the results from Ref. 22 for the first-excited-state energies for coverages greater than 0.10 Å^{-2}. The agreement with experiment is excellent except in the region close to the layering transition. We should also note that in Ref. 24 measurements were extended into the very-low-^{4}He-coverage region below 0.07 Å^{-2} in Fig. 1. In this region, our first-

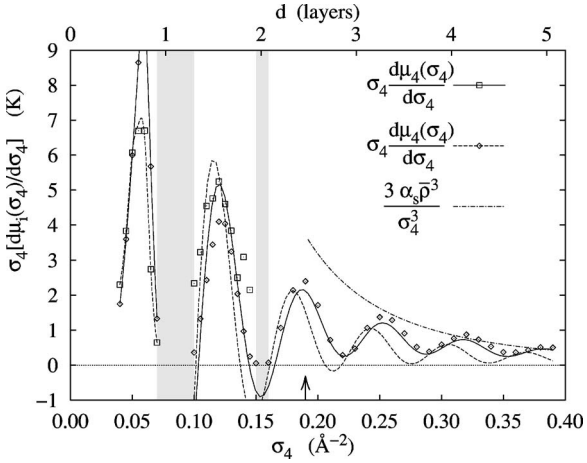

FIG. 3. The calculated incompressibilities $m_4c_3^2$ of ^{4}He on the Nuclepore substrate as calculated from the long-wavelength limit of the excitations—i.e., from Eq. (2.36) with the HNC approximation (2.25) for the particle-hole interaction (diamonds). Also shown are the results obtained by differentiating the fit (3.5) (solid line) and the asymptotic forms (3.6) (short-long-dashed line). The figure also shows the corresponding quantity $\sigma(d\mu_3/d\sigma)$ obtained from the long-wavelength limit of the particle-hole interaction [Eq. (2.45), boxes] and from differentiating the fit (3.5) (dashed line). The gray areas are regimes of layering transitions. The solid and dashed lines connecting the points in the first layer are not part of the fit (3.5) but a spline of the data to guide the eye. The arrow located at 0.19 Å^{-2} is our best estimate for the mobile film coverage corresponding to the experiment of Sheldon and Hallock (Ref. 5). The upper scale gives the thickness of the films in *liquid* layers; one ^{4}He layer is defined as representing an areal density of 0.077 Å^{-2}.

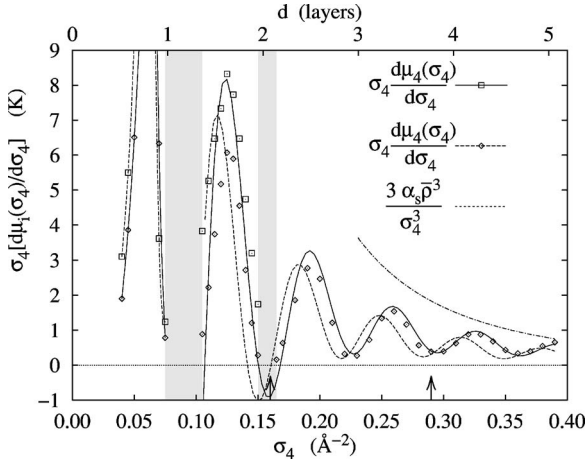

FIG. 4. Same as Fig. 3 for the glass substrate. The arrows located at 0.16 and 0.29 Å^{-2} are our best estimates for the mobile film coverage corresponding to the experiment of Valles, Heinrichs, and Hallock (Ref. 7).

excited-state energies are in reasonable agreement with experiment; however, the ground-state energies are in strong disagreement. The experimental numbers are approximately coverage independent at ≈ -5.2 K, whereas, as seen in Fig. 1, the theoretical results decrease strongly with decreasing film thickness. In the following, we shall be mainly concerned with the region beyond the first-layering transition where calculation and experiment are in good agreement.

The ^{3}He energetics are quite similar between the Nuclepore and glass systems at the coverages corresponding to experiment. The ^{3}He level spacing (magnitude of the difference between the first-excited-state and ground-state single-particle energies) for the Nuclepore system at 0.19 Å^{-2} is 2.2 K, and for the glass system it is 2.2 K at 0.165 Å^{-2} and 2.3 K at 0.290 Å^{-2}. We note in passing that there is considerable experimental evidence that, for the Nuclepore system, the adsorbed ^{3}He begins occupying the first excited state prior to monolayer completion.[25] The evidence includes recent heat capacity measurements by Ho and Hallock.[26] The calculated Nuclepore level spacing of 2.2 K is just below the estimated Fermi energy at monolayer completion of 2.3 K. This result is an improvement from past calculations which have tended to yield level spacings larger than the estimated Fermi energy at monolayer completion. However, it is not yet in quantitative agreement with experiments that show first excited occupation at approximately 0.6 of a ^{3}He monolayer.

We now examine the ^{4}He incompressibilities $m_4c_3^2$ shown in Figs. 3 and 4 for Nuclepore and glass, respectively. As discussed above, there are two ways that one can calculate the third-sound speeds. First, one can calculate the derivative (2.30) of the fitting function (3.5). These results are shown as solid lines. This corresponds to evaluating the expression (2.36) with the particle-hole interaction defined by the second variation (2.32). Second, one can obtain the incompressibility from long-wavelength excitations—i.e., with the particle-hole interaction taken from Eq. (2.25). These results are shown by diamond symbols. To assess the quality of the agreement, we should recall that the small value of $m_4c_3^2$ is actually due to large-scale cancellations. A *typical* value of the particle-hole potential throughout the film is of the order of m_4c^2, where c is the first-sound speed—i.e., of the order of 30 K. Only the very specific combination (2.36) gives the speed of the *surface excitation* which should go to zero in the thick-film limit. There is no diagrammatic reason that this should be the case; hence, the small value of Eq. (2.36) *per se* supports strongly our calculational procedure. In that sense, the agreement between the incompressibilities calculated in different ways is quite satisfactory.

The dash-dotted lines in Figs. 3 and 4 show the asymptotic incompressibilities obtained from the first two terms of the fit (3.5). It is even more evident than in the previous comparison of the chemical potentials that our highest coverage film barely approaches the thickness where asymptotic power laws are valid.

The situation is somewhat different for the calculations involving properties of the ^{3}He impurities. For technical reasons one obtains somewhat larger numerical uncertainties for thicker films. The calculated values as well as the fits of the mixed quantities $\sigma_4 d\mu_3/d\sigma_4$ needed for the third-sound analysis, Eq. (3.2), are shown in Figs. 3 and 4 in the coverage regime $\sigma_4 > 0.10$ Å^{-2}. From these fits we have obtained the energy of the Andreev state in the bulk limit of -5.23 K for Nuclepore and -5.17 K for the glass substrate, in good agreement with experiment.[27]

The other coefficients that should be comparable to those of the background calculation; specifically the van der Waals

term and the oscillatory part of the density, are reasonably consistent. Recall that our results indicate that the films under consideration here are still far from the thickness where the chemical potential is dominated by the van der Waals term. Consequently, one cannot expect that a fit of the results in the regime $0.010\ \text{Å}^{-2} < \sigma_4 < 0.40\ \text{Å}^{-2}$ reproduces this term accurately. For example, for Nuclepore, the fit (3.5) suggests an average density $\bar{\rho}=0.019\ \text{Å}^{-3}$, whereas the glass substrate suggests $\bar{\rho}=0.023\ \text{Å}^{-3}$.

From the oscillatory part of the representation (3.5) one can also get an estimate of the layer thickness. All four fits lead to values of the parameter k between 95 Å^2 and 100 Å^2, suggesting a layer thickness of 0.066 Å^{-2} which is in reasonable agreement with the "conventional" value of 0.077 Å^{-2}.

The calculation of $\sigma_4 d\mu_3(\sigma_4)/d\sigma_4$ from Eq. (2.45) is much less reliable than the calculation of $\sigma_4 d\mu_4(\sigma_4)/d\sigma_4$. The hydrodynamic derivative agrees with the microscopic derivative (2.45) only for single- and double-layer configurations.

Figures 3 and 4 show that the third-sound speed oscillates in parallel with the layered structure of the ^{4}He film. As far as we know, this effect has not yet been seen. In the regions of the layering transitions, the physical third-sound speeds are determined by Maxwell-type constructions that are not shown in the figures. But note that the oscillations are clear even beyond the regions of the layering transitions.

Even more interesting is the effect of a small amount of ^{3}He on the third-sound speed as predicted by Eq. (3.2) or (3.3). By inspection of Figs. 3 and 4, we see that the slope of $d\mu_3/d\sigma_4$ *changes sign* in the region of the oscillations. Thus, a further prediction of these calculations is that, for thin ^{4}He films on substrates such as Nuclepore or glass, regions may be found in which the third-sound speed *increases* as a function of added ^{3}He.

While the qualitative scenario is quite clear, we would like to be cautious with quantitative statements. It appears to be clear that the ^{3}He chemical potential has, just like the ^{4}He chemical potential, a sizable oscillatory behavior. Taking higher derivatives, this oscillatory behavior is enhanced relative to the smooth, power-law behavior. Moreover, taking the coverage derivative of the oscillatory part causes a 90° phase shift of the oscillations; note that the oscillations of the ^{4}He and ^{3}He chemical potentials are almost in phase.

The evaluation of Eq. (3.2) requires, on the other hand, the calculation of a second derivative of a function that has been obtained from a fit to numerical data which contain some uncertainties. Instead of examining the quantity Δ defined in Eq. (1.3) we have therefore calculated, using Eq. (3.2), the total incompressibility. This quantity is composed of the sum of the ^{4}He incompressibilities, as shown in Figs. 3 and 4, plus an added contribution due to the ^{3}He in the low-concentration, linear limit. The result is shown in Fig. 5 for the Nuclepore system. To the extent that the linearization of the ^{3}He dependence of the incompressibility is legitimate, the results are quite interesting. They quantify, of course, the above statement that, depending on the ^{4}He coverage, the incompressibility may increase or decrease with ^{3}He concentration. In the vicinity of layering transitions, the effect can be strong enough to make the film unstable. The effect is particularly pronounced in the triple-layer films with coverages between 0.165 Å^{-2} and 0.22 Å^{-2}: In the lower half of that coverage regime, the addition of ^{3}He would have the tendency to *stabilize* the films, whereas it *destabilizes* the translationally invariant configuration at coverages above 0.19 Å^{-2}. This is consistent with the drop in the speed of sound seen in Ref. 5. Of course, inspection of Fig. 5 shows clearly that the drop in third-sound speed depends quite sensitively on the coverage and a quantitative comparison is not feasible. As the coverage is further increased, the ^{4}He film can actually undergo a layering transition; this happens, in our model, at modest ^{3}He concentrations of 0.25 monolayers at a ^{4}He coverage of about 0.21 Å^{-2}. The configuration of the film in this regime would be a mixture of regions that would consist of three layers of ^{4}He without ^{3}He in Andreev states and double layers of ^{4}He with ^{3}He in surface states.

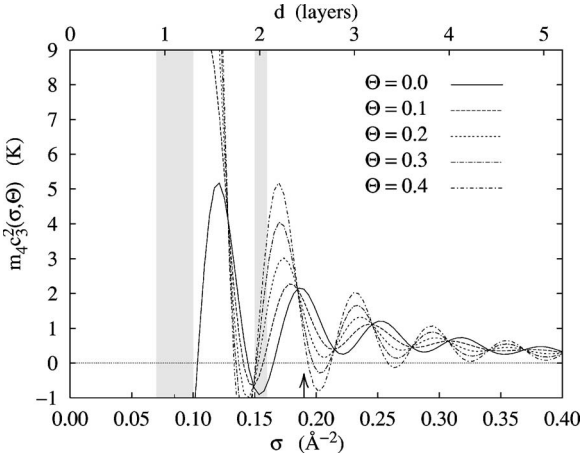

FIG. 5. On the same scale as Fig. 3, the total incompressibility of the mixture film on Nuclepore as a function of ^{3}He coverage in the low-concentration regime, as given by Eq. (3.2). The arrow located at 0.19 Å^{-2} is our best estimate for the mobile film coverage corresponding to the experiment of Sheldon and Hallock (Ref. 5).

B. Structure

Our examination of the energetics of both ^{4}He background and ^{3}He impurity indicates clearly that the properties of both species are far from monotonic functions of the film thickness. The basic reason for this is the layered growth of the background film which is a direct consequence of both the hard core of the ^{4}He-^{4}He interaction and the strength of the substrate potential. This is, of course, also reflected in the ^{3}He probability density. In Fig. 6, we show the ^{3}He ground-state (solid lines) and first-excited-state (dashed lines) density profiles for a series of ^{4}He film coverages on Nuclepore. The largest coverage shown corresponds to our estimate of the mobile film coverage ($\sigma_4 \approx 0.19$) for the Sheldon-Hallock experiment.[5]

At the very lowest ^{4}He coverages, the ^{3}He ground-state density profile corresponds almost exactly with the ^{4}He profile. This is simple to understand. If there is only a small amount of mobile ^{4}He, then the ^{3}He can lower its total energy by moving as close to the substrate as possible without

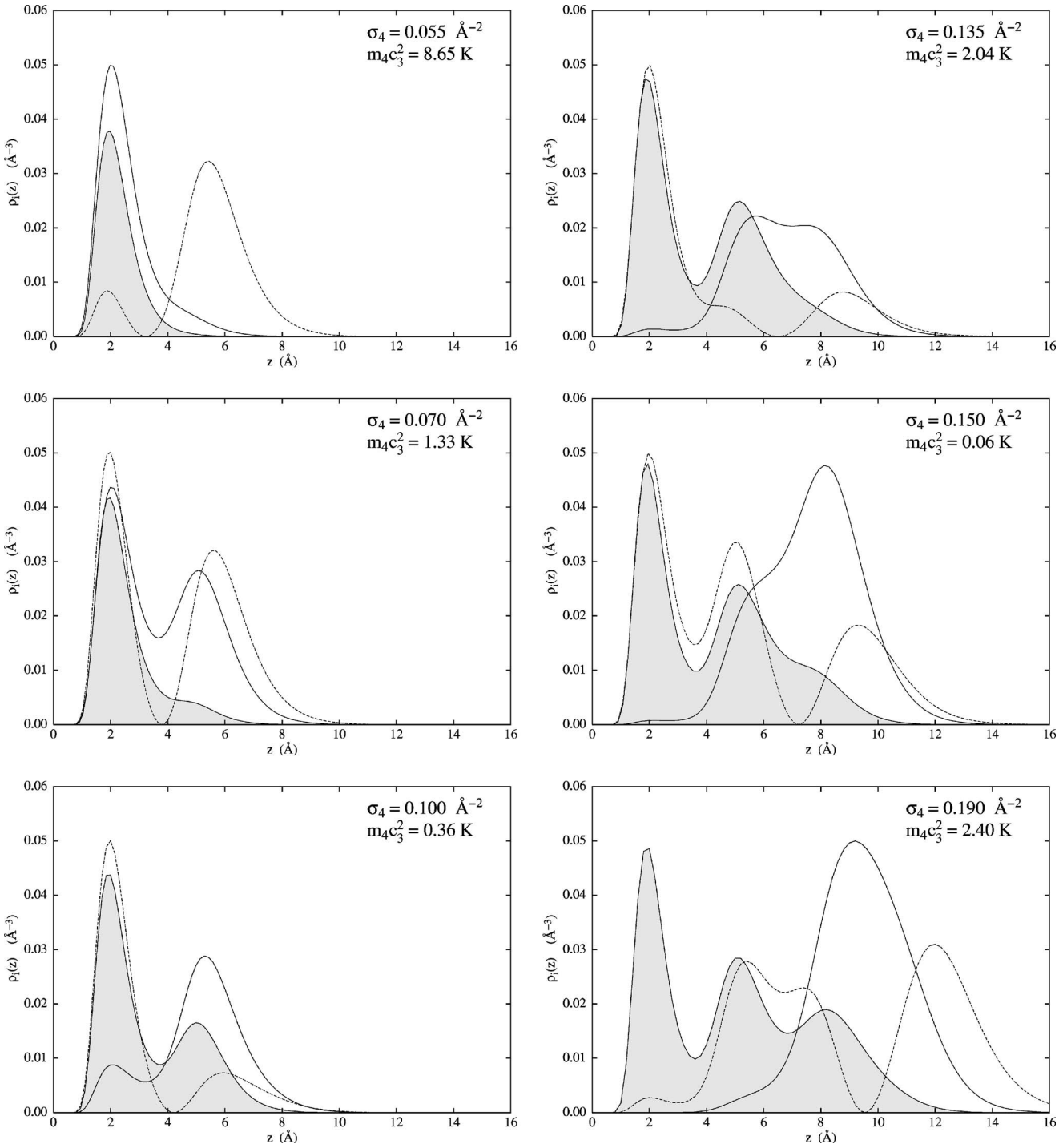

FIG. 6. The density profiles of the ^{4}He background (gray shaded area), the ^{3}He ground state (solid line), and the first excited state (dashed line) in a number of typical situations on the Nuclepore substrate. The normalization of the ^{3}He densities is arbitrary. The coverage for the final figure, σ_4=0.19 Å^{-2}, corresponds to the experiment of Sheldon and Hallock (Ref. 5). At this stage, the ^{3}He adatom is in a well-defined Andreev state. The probability density for the first excited state is fairly equally distributed between being in the film and outside of the film.

a large cost in correlational kinetic energy. As ^{4}He is added to the system, however, the cost in kinetic energy to the ^{3}He begins to rise and so the ^{3}He reacts by moving towards the free surface of the ^{4}He film. At the coverage of the experiment, the ^{3}He is in a well-formed Andreev-like state (with a full width at half height that is approximately 3.9 Å which is the conventional ^{3}He layer thickness ℓ_3).

This gradual motion of the ^{3}He from "mixed" in the ^{4}He film to "separated" from the ^{4}He film, as a function of increasing ^{4}He coverage, was first observed experimentally on a Nuclepore substrate by Noiray *et al.*[8] They termed it a "stratification transition" but as seen in Fig. 6 this is not a sudden motion from mixed to separated but simply a gradual evolution.

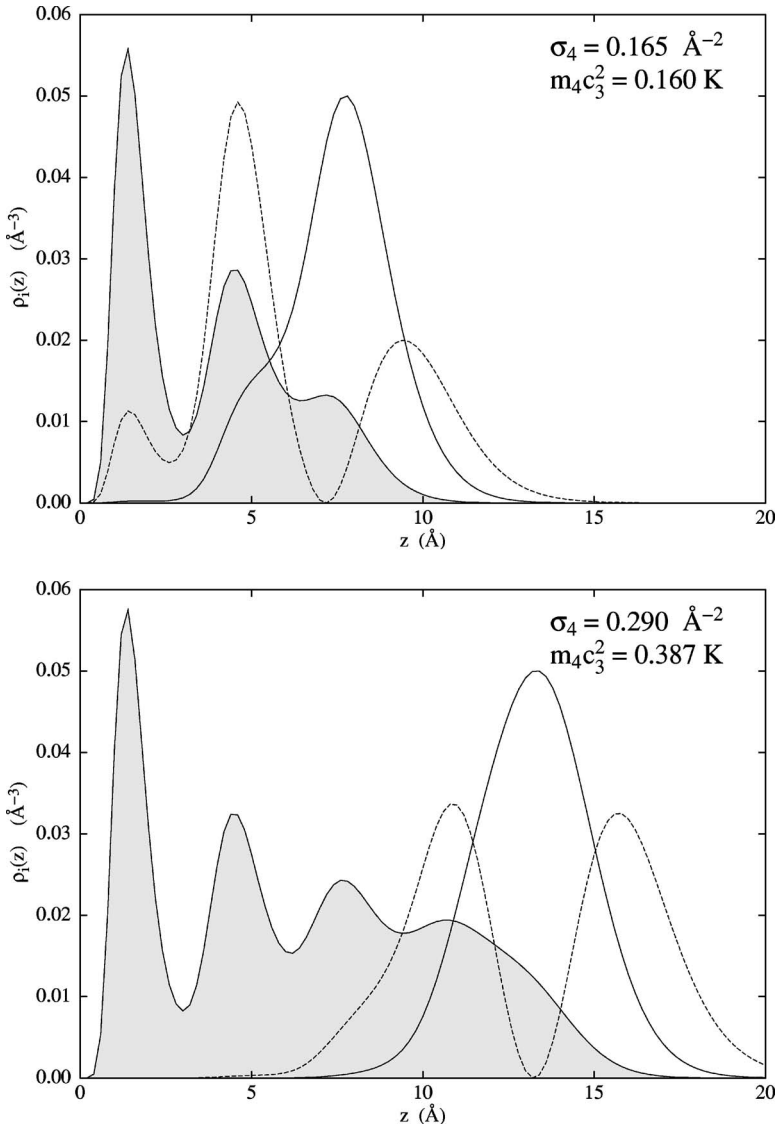

FIG. 7. Same as Figs. 6 for the glass substrate at the coverages relevant to the experiments of Ref. 7. Observe that the horizontal scale is different from Fig. 6.

Figure 6 also shows the ^{3}He first-excited-state probability densities. The evolution of these states is complementary to that of the ground states because of the requirement of orthogonalization. At low ^{4}He film coverages, the first-excited-state probability density is located preferentially outside of the ^{4}He film, and as the ground-state probability shifts out with increasing ^{4}He coverage, the first excited state shifts in. By the largest coverage shown, the probability distribution for the first excited state is roughly half in and half out of the ^{4}He film. The occupation of the first excited state as a function of ^{3}He coverage is considered a possible path to second-layer formation (of the ^{3}He on the ^{4}He film).[25] Clearly, in order for this view to be sensible, the present trend must be reversed with increasing ^{3}He coverage. That is, as a function of ^{3}He coverage, we expect to see the first excited state begin to emerge from the ground state on the free-surface side where second-layer formation should appear. This latter calculation is far beyond the scope of this work.

In Fig. 7, we show the ^{3}He ground-state and first-excited-state probability densities at the coverages 0.165 Å^{-2} and 0.290 Å^{-2}, which correspond to the mobile film coverages in the experiment of Ref. 7 on the glass substrate. The lower-coverage results, which we do not show in order to save some space, mimic those of the Nuclepore substrate shown above in Fig. 6. For the same reasons as for Nuclepore, this system also exhibits a gradual "stratification" transition. At submonolayer coverages, the ^{3}He and ^{4}He probability densities overlap, and as the ^{4}He coverage is increased the ^{3}He ground state is pushed out of the film into a surface state. The results shown in Fig. 7 are qualitatively similar to the Nuclepore results at 0.190 Å^{-2}. There are well-defined Andreev-like states for both coverages. The most obvious small difference is at the lower coverage where the first-excited-state density is preferentially located on the ^{4}He-film side.

IV. CONCLUSION

In this paper we have utilized first-principles, microscopic calculations to determine the hydrodynamic response of pure ^{4}He films and ^{4}He films with a small amount of adsorbed ^{3}He on Nuclepore and glass model substrates. Our goal was to try to understand the experiments that have been done on these systems and to test the applicability of film-averaged

hydrodynamic models. Our results can be summarized as follows.

(i) The most important results from our microscopic analysis of the mixture-film third-sound speeds are shown in Figs. 5 and 3. These results show that, for a thin, layered film, the third-sound speeds can have dramatic film-coverage dependence and that, in regions where the pure third-sound speed is small, the contributions from the ^{3}He component can have critically important effects. It is our conclusion then that the experimental results of Refs. 5 and 7 are sensitive to the choice of ^{4}He film thickness and that different results may have been seen with slightly different changes in coverage.

(ii) The layered structure of the ^{4}He film induces coverage-dependent ^{3}He and ^{4}He chemical potentials that in turn yield nonmonotonic third-sound speeds as a function of ^{4}He film coverage. This response should be observable in thin films on strong substrates. In recent work, we have shown that these results are also valid for the weakly interacting substrates Li and Na.[28]

(iii) We have shown that in some ranges of ^{4}He film thickness, the addition of small amounts of ^{3}He is able to destabilize a laterally homogeneous film and create patches of ^{3}He rich and ^{3}He poor regions. We further note that phase separation has been reported in thin mixture films by Bhattacharyya and Gasparini[29] on Nuclepore and Csáthy, Kim, and Chan[30] on H_2-plated gold. It is intriguing to note that the anomalous mixture film system investigated by Bhattacharyya and Gasparini had a coverage ≈ 0.26 Å^{-2}; this value is located in a possibly unstable region as shown in Fig. 5.

(iv) For thin films, the film-averaged hydrodynamic formulas are in *qualitative* disagreement with the microscopic results. The formulas can be made to fit particular results with sufficient effort at modeling.

(v) The microscopic calculations also predict regions in which the third-sound speed will increase with the addition of small amounts of ^{3}He. This response also should be observable in thin films on strong substrates.

(vi) The stratification transition of Ref. 8 is clearly seen on both the Nuclepore and glass results. It is easily explained by noting that the ^{3}He can minimize its energy in a submonolayer ^{4}He film by moving as close to the substrate as possible, and it will minimize its energy for multilayer ^{4}He films by moving to the the film surface. This evolution is a smooth function of the ^{4}He coverage.

The dissimilarities in the low-^{3}He-coverage dependence of the third-sound responses on Nuclepore and glass are striking when one considers how similar the ground-state probability densities and level spacings are. These results imply that the question of the extent of a linear region in the incompressibility cannot be answered in the single-^{3}He-atom limit and may require detailed knowledge of the ^{3}He effective interaction in the environment of a thin ^{4}He film.

There are some further ramifications for third-sound experiments. In the *thin-film* limit, for substrates that induce a significant layered structure, the concept of a ^{4}He film thickness d is ambiguous. The only nonambiguous measure of film thickness is the areal density or coverage. Thus, in order to minimize ambiguity, reports of thin-film experiments on strong substrates need to provide both the areal density of the immobile layer and the areal density of the total film. For purposes of illumination, one can also provide "film thicknesses" by dividing the coverage by the bulk density but such a number does not have any fundamental significance.

We should add that our conclusion concerning the inapplicability of film-averaged hydrodynamic models to *these systems* is not the same as saying that hydrodynamics is *generally* inapplicable. Third sound is a well-defined hydrodynamic mode, and if one pursues the theory allowing nontrivial substrate-normal density oscillations, then one can presumably improve the existing thick-film theory.

ACKNOWLEDGMENTS

M.D.M. would like to express his appreciation to the Institute for Theoretical Physics at Johannes-Kepler University for support during the period of a professional leave.

APPENDIX

In this appendix, we examine the fundamental Maxwell identity, Eq. (3.4), from both macroscopic and microscopic points of view.

The ^{3}He and ^{4}He chemical potentials are defined by

$$\mu_3 = \left(\frac{\partial G}{\partial \mathcal{N}_3}\right)_{\mathcal{N}_4,\mathcal{P},\mathcal{T}}, \tag{A1}$$

$$\mu_4 = \left(\frac{\partial G}{\partial \mathcal{N}_4}\right)_{\mathcal{N}_3,\mathcal{P},\mathcal{T}}, \tag{A2}$$

where G is the Gibbs free energy. From Eqs. (A1) and (A2) we immediately obtain the Maxwell relation

$$\left(\frac{\partial \mu_4}{\partial \mathcal{N}_3}\right)_{\mathcal{P},\mathcal{T}} = \left(\frac{\partial \mu_3}{\partial \mathcal{N}_4}\right)_{\mathcal{P},\mathcal{T}}. \tag{A3}$$

We use the identity

$$\left(\frac{\partial \mu_4}{\partial \mathcal{N}_3}\right)_{\mathcal{A},\mathcal{T},\mathcal{N}_4} = \left(\frac{\partial \mu_3}{\partial \mathcal{N}_4}\right)_{\mathcal{P},\mathcal{T},\mathcal{N}_4} + \left(\frac{\partial \mu_4}{\partial \mathcal{P}}\right)_{\mathcal{N}_3,\mathcal{T},\mathcal{N}_4}\left(\frac{\partial \mathcal{P}}{\partial \mathcal{N}_3}\right)_{\mathcal{A},\mathcal{T},\mathcal{N}_4}$$
$$= \left(\frac{\partial \mu_3}{\partial \mathcal{N}_4}\right)_{\mathcal{P},\mathcal{T},\mathcal{N}_4} + \frac{a_3 a_4}{\mathcal{A}\beta_{\mathcal{T}}}, \tag{A4}$$

where a_3 and a_4 are partial areas and $\beta_{\mathcal{T}}$ is the isothermal compressibility. Since the second term in Eq. (A4) is symmetric in 3 and 4, Eq. (3.4) is proved.

We also need to examine to what extent Eq. (3.4) is obeyed by the microscopic theory. In keeping with the spirit of this paper, we derive explicit expressions for the density derivatives of the chemical potentials in the limit of low ^{3}He coverage. The density functions are determined by the "Hartree" equations (2.28) and (2.42), respectively:

$$\left[-\frac{\hbar^2}{2m_i}\nabla^2 + U_{\text{ext}}(\mathbf{r}) + V_{\text{H}}^{(i)}(\mathbf{r})\right]\sqrt{\rho_i(\mathbf{r})} = \mu_i\sqrt{\rho_i(\mathbf{r})}, \tag{A5}$$

where $i=3,4$ and

$$V_{\rm H}^{(i)}(\mathbf{r}) = \frac{\delta E_{\rm c}[\rho_3,\rho_4]}{\delta\rho_i(\mathbf{r})}. \tag{A6}$$

We now use Eq. (A5) to calculate density derivatives of the chemical potentials.

Analogous to Eq. (2.31), the σ_3 derivative is

$$\left[-\frac{\hbar^2}{2m_4}\nabla^2 + U_{\rm ext}(\mathbf{r}) + V_{\rm H}^{(4)}(\mathbf{r}) - \mu_4\right]\frac{d\sqrt{\rho_4(\mathbf{r})}}{d\sigma_3} + \frac{dV_{\rm H}^{(4)}(\mathbf{r})}{d\sigma_3}\sqrt{\rho_4(\mathbf{r})} = \frac{d\mu_4}{d\sigma_3}\sqrt{\rho_4(\mathbf{r})}, \tag{A7}$$

and

$$\frac{dV_{\rm H}^{(4)}(\mathbf{r})}{d\sigma_3} = \int d^3r'\left[V_{\text{p-h}}^{(44)}(\mathbf{r},\mathbf{r}')\frac{d\rho_4(\mathbf{r}')}{d\sigma_3} + V_{\text{p-h}}^{(43)}(\mathbf{r},\mathbf{r}')\frac{d\rho_3(\mathbf{r}')}{d\sigma_3}\right]. \tag{A8}$$

As above, these equations can be combined to yield

$$\int d^3r'[H_1^{(4)}(\mathbf{r})\delta(\mathbf{r}-\mathbf{r}') + 2\tilde{V}_{\text{p-h}}^{(44)}(\mathbf{r},\mathbf{r}')]\frac{d\sqrt{\rho_4(\mathbf{r}')}}{d\sigma_3} + \int d^3r' 2\tilde{V}_{\text{p-h}}^{(43)}(\mathbf{r},\mathbf{r}')\frac{d\sqrt{\rho_3(\mathbf{r}')}}{d\sigma_3} = \frac{d\mu_4}{d\sigma_3}\sqrt{\rho_4(\mathbf{r})}. \tag{A9}$$

Now multiply Eq. (A9) by $d\sqrt{\rho_4(\mathbf{r})}/d\sigma_3$ and integrate to yield

$$\frac{d\mu_4}{d\sigma_4}\int d^3r\sqrt{\rho_4(\mathbf{r})}\frac{d\sqrt{\rho_4(\mathbf{r})}}{d\sigma_3} + 2\int d^3r d^3r'\frac{d\sqrt{\rho_4(\mathbf{r})}}{d\sigma_4}\times\tilde{V}_{\text{p-h}}^{(43)}(\mathbf{r},\mathbf{r}')\frac{d\sqrt{\rho_3(\mathbf{r})}}{d\sigma_3} = \frac{d\mu_4}{d\sigma_3}\int d^3r\sqrt{\rho_4(\mathbf{r})}\frac{d\sqrt{\rho_4(\mathbf{r})}}{d\sigma_4}. \tag{A10}$$

The first term vanishes, and the right hand-side is simply $(1/2)d\mu_4/d\sigma_3$. Finally, if we assume that the ^{3}He ground state can be written $\rho_3(\mathbf{r}) = |\psi_3(z)|^2\sigma_3$, then $d\rho_3/d\sigma_3 = \rho_3/\sigma_3$ and we find

$$\sigma_3\frac{d\mu_4}{d\sigma_3} = 2\int d^3r d^3r'\frac{d\sqrt{\rho_4(\mathbf{r}')}}{d\sigma_4}\tilde{V}_{\text{p-h}}^{(43)}(\mathbf{r},\mathbf{r}')\sqrt{\rho_3(\mathbf{r})}, \tag{A11}$$

in agreement with Eq. (2.45).

*Electronic address: eckhard.krotscheck@jku.at
†Electronic address: mdm@wsu.edu

[1] D. J. Bergman, in *Physical Acoustics: Principles and Methods*, edited by W. P. Mason and R. N. Thurston (Academic, New York, 1975), Vol. XI.
[2] F. M. Ellis, R. B. Hallock, M. D. Miller, and R. A. Guyer, Phys. Rev. Lett. **46**, 1461 (1981).
[3] R. A. Guyer and M. D. Miller, Phys. Rev. B **25**, 5749 (1982).
[4] R. H. Anderson, M. D. Miller, and R. B. Hallock, Phys. Rev. B **59**, 3345 (1999).
[5] P. A. Sheldon and R. B. Hallock, Phys. Rev. B **50**, 16082 (1994).
[6] R. H. Anderson and M. D. Miller, J. Low Temp. Phys. **116**, 85 (1999).
[7] J. M. Valles, R. M. Heinrichs, and R. B. Hallock, Phys. Rev. Lett. **56**, 1704 (1986).
[8] J. C. Noiray, D. Sornette, J. P. Romagnan, and J. P. Laheurte, Phys. Rev. Lett. **53**, 2421 (1984).
[9] D. T. Sprague, N. Alikacem, and R. B. Hallock, Phys. Rev. Lett. **74**, 4479 (1995).
[10] R. H. Higley, D. T. Sprague, and R. B. Hallock, Phys. Rev. Lett. **63**, 2570 (1989).
[11] J. H. Scholtz, E. O. McLean, and I. Rudnick, Phys. Rev. Lett. **32**, 147 (1974).
[12] E. S. Sabisky and C. H. Anderson, Phys. Rev. A **7**, 790 (1973).
[13] V. Apaja and E. Krotscheck, in *Microscopic Approaches to Quantum Liquids in Confined Geometries*, edited by E. Krotscheck and J. Navarro (World Scientific, Singapore, 2002), pp. 205–268.
[14] T. Morita and K. Hiroike, Prog. Theor. Phys. **25**, 537 (1960).
[15] E. Krotscheck, in *Microscopic Quantum Many-Body Theories and their Applications*, Vol. 510 of Lecture Notes in Physics, edited by J. Navarro and A. Polls (Springer, Heidelberg, 1998), pp. 187–250.
[16] E. Krotscheck, G.-X. Qian, and W. Kohn, Phys. Rev. B **31**, 4245 (1985).
[17] B. E. Clements, E. Krotscheck, and M. Saarela, Phys. Rev. B **55**, 5959 (1997).
[18] E. Feenberg, *Theory of Quantum Fluids* (Academic, New York, 1969).
[19] C. E. Campbell, in *Progress in Liquid Physics*, edited by C. A. Croxton (Wiley, London, 1977), Chap. 6, pp. 213–308.
[20] J. W. Clark, in *Progress in Particle and Nuclear Physics*, edited by D. H. Wilkinson (Pergamon, Oxford, 1979), Vol. 2, pp. 89–199.
[21] E. Krotscheck, Phys. Rev. B **32**, 5713 (1985).
[22] D. T. Sprague, N. Alikacem, P. A. Sheldon, and R. B. Hallock, Phys. Rev. Lett. **72**, 384 (1994).
[23] N. Alikacem, D. T. Sprague, and R. B. Hallock, Phys. Rev. Lett. **67**, 2501 (1991).
[24] P. A. Sheldon and R. B. Hallock, Phys. Rev. Lett. **77**, 2973 (1996).
[25] R. H. Anderson and M. D. Miller, in *Condensed Matter Theories*, edited by J. W. Clark and R. M. Panoff (Nova Science, Hauppauge, NY, 2005), Vol. 20.
[26] P.-C. Ho and R. B. Hallock, Phys. Rev. Lett. **87**, 135301 (2001).
[27] D. O. Edwards and W. F. Saam, in *Progress in Low Temperature Physics*, edited by D. F. Brewer (North-Holland, New York, 1978), Vol. 7A, Chap. 4, pp. 282–369.
[28] E. Krotscheck and M. D. Miller, J. Low Temp. Phys. **141**, 1 (2005).
[29] B. Bhattacharyya and F. M. Gasparini, Phys. Rev. Lett. **49**, 919 (1982).
[30] G. A. Csáthy, E. Kim, and M. H. W. Chan, Phys. Rev. Lett. **88**, 045301 (2002).